IOP Publishing Journal of Physics B: Atomic, Molecular and Optical Physics
J. Phys. B: At. Mol. Opt. Phys. **53** (2020) 184006 (8pp) https://doi.org/10.1088/1361-6455/aba1ca

Electronic decay through non-linear carbon chains

John B Mullenix[1], Victor Despré[1,3] and Alexander I Kuleff[1,2]

[1] Theoretische Chemie, Universität Heidelberg, Im Neuenheimer Feld 229, 69120 Heidelberg, Germany
[2] ELI-ALPS, W. Sandner utca 3, 6728 Szeged, Hungary

E-mail: victor.despre@pci.uni-heidelberg.de and alexander.kuleff@pci.uni-heidelberg.de

Received 10 February 2020, revised 29 April 2020
Accepted for publication 1 July 2020
Published 24 July 2020

Abstract

A multielectron wave-packet propagation method was used to calculate the electronic decay of oxygen and fluorine 2*s* vacancies for a group of trifluoroalkyl alcohols, $HOC_nH_{(2n-1)}F_3$, with *n* between 1 and 5. Whether ionizing O2*s* or F2*s* orbitals, it is shown that an electron can be emitted non-locally from the opposite terminus of the molecule. The decay of the $O(2s^{-1})$ state is found to be about 2–3 times faster than that of the $F(2s^{-1})$, but in both cases the process takes only a few femtoseconds, demonstrating a highly efficient energy transfer through the carbon bridge. A comparison to the previously reported non-local decay in linear difluorocumulenone systems shows that the non-linearity of the trifluoroalkyl alcohols does not appear to dramatically influence the decay efficiency. These results shed light onto the nature of the scaling of electron correlation and open the door to the potential design of molecules that take advantage of this mechanism.

Keywords: non-local decay, ultrafast electron dynamics, electron correlation, carbon chains

(Some figures may appear in colour only in the online journal)

1. Introduction

In recent years, dramatic progress in attosecond spectroscopy has enabled the experimental observation of effects for which electron correlation plays a crucial role [1, 2]. Among others, we can cite observations of charge localization [3], photoemission delay [4], instantaneous dipole moment [5], and pure electronic dynamics [6, 7]. The ultrafast, non-Born–Oppenheimer relaxation of highly excited cationic states has also been observed in a series of medium-sized molecules [8–13], and the strong electron correlation was recognized [9, 12, 13] as a crucial factor for determining the excited state dynamics in complex systems. Another important mechanism driven by electron correlation is the electronic decay. After ionization of a core or deep inner-valence orbital of an atom, the created vacancy can be filled by a higher-lying electron, which results in the emission of a second electron. Depending on which electronic shells participate in the transition, the process is referred to as Auger decay [14, 15], Coster–Kronig [16] and super Coster–Kronig [17] transitions. The typical timescale of this very efficient process is in the femtosecond range [18], or even attosecond range [19] for super Coster–Kronig transitions.

These electronic decay mechanisms also appear in more complex systems such as molecules or clusters. The decay of deep-core holes still proceeds mostly locally, i.e. involves electrons 'belonging' to the atom bearing the initial vacancy. The situation changes dramatically when an inner-valence hole is created. In this case, due to the correlation between more delocalized valence electrons, the decay may proceed non-locally, involving electrons 'belonging' to remote atoms or subunits. Due to the long-range Coulomb interaction, the electron correlation is operative over large distances and can drive decay transitions even between weakly interacting, separate species in a process known as interatomic/intermolecular Coulombic decay (ICD) [20]. In this mechanism, extensively studied both theoretically (see, e.g. references [21–24]) and experimentally (see, e.g. references [25–30]), the relaxation of the initially

[3] Author to whom any correspondence should be addressed.

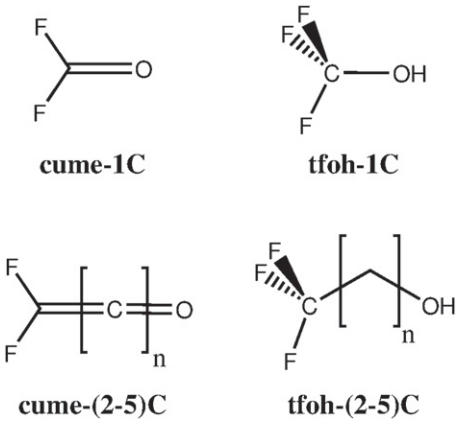

Figure 1. Left: difluorocumulenones studied in reference [33]. Right: trifluoroalkyl alcohols studied in this report. Labeling follows the rule **cume-*n*C** or **tfoh-*n*C** for the difluorocumuleones or trifluoroalkyl alcohols, respectively, where *n* corresponds to the number of carbons.

excited species occurs by transferring its excess energy to a weakly bound neighbor, which emits an electron.

In order to understand non-local decay, one must assess how its efficiency is affected by the distance between two subunits involved in the transition. In ICD, this can be conceptualized using a virtual-photon model [31], in which the decay is described by a dipole–dipole interaction between the two units, and the decay efficiency decreases as R^{-6} with the distance R between the interacting species [32]. The virtual-photon model, however, cannot be transferred to chemically bound systems, for which it drastically underestimates the decay time. How ICD compares to intramolecular non-local decay of valence hole states in bound systems remains mostly unexplored.

Our first foray into such a study was reported recently [33]. The non-local intramolecular decay following inner-valence ionization was calculated for a series of difluorocumulenones (see figure 1). Cumulenes are unsaturated chains of carbon atoms. The difluorocumulenones studied in our first work consisted of a chain of 1–5 *sp*-hybridized carbon atoms, capped by a carbonyl group on one end and two symmetrically equivalent fluorine atoms on the opposite end. We showed that in such systems an O($2s^{-1}$) vacancy can decay non-locally by emitting an electron from the remote fluorines with a time constant that increases almost linearly with the O–F_2 distance. This is orders of magnitude faster than the R^{-6} dependence expected in an ICD type of transition, indicating that the energy transfer through bonds proceeds much faster than through 'empty' space. In this respect, it is interesting to study how the efficiency of the energy transfer depends on the type of chemical bonding, which might round out our understanding of the process and, more generally, of the electronic correlation.

With this aim in mind, we have studied fully saturated primary alkyl alcohols with three fluorine atoms collected on the end opposite the hydroxyl group (see figure 1). There are three goals behind this choice of system. First, they provide a non-linear backbone for the energy propagation, which can be contrasted to the linear cumulenones examined previously, shedding light on possible size effects arising from the electron correlation. A size effect for the electron correlation has also been recently reported for correlation-driven charge migration [34, 35] in a series of alkyne chains [36]. The study of this size effect can pave the way to electron-correlation-based molecular design, with application in molecular-scale electronics, for which carbon chains can be used as bridges [37]. Second, the synthesis of alkyl alcohols is easier than preparing extended cumulenones, which opens the door to eventual experimental follow-up. Third, the energy propagation will be studied in both directions, with separate calculations for either oxygen or fluorine bearing the initial hole. This latter goal should help to better understand the role played by the different functional groups participating in the non-local decay and their interaction through the mediating bridge.

2. Theoretical background

The decay dynamics were obtained by computing the time-dependent hole density, which is defined as the difference between the electron densities of the molecule before and after ionization [34, 38]:

$$\begin{aligned} Q(\vec{r},t) &:= \langle\Psi_0|\hat{\rho}(\vec{r},t)|\Psi_0\rangle - \langle\Psi_i|\hat{\rho}(\vec{r},t)|\Psi_i\rangle \\ &= \rho_0(\vec{r}) - \rho_i(\vec{r},t). \end{aligned} \tag{1}$$

In the above expression, $|\Psi_0\rangle$ and $|\Psi_i\rangle$ refer to the neutral ground state and the initially prepared cationic state, respectively, while $\hat{\rho}$ is the electron density operator. Thus, $\rho_0(\vec{r})$ represents the time-independent electron density of the neutral molecule in its ground state, and the time-dependent electron density is given by

$$\begin{aligned} \rho_i(\vec{r},t) &= \langle\Psi^{N-1}(0)|\mathrm{e}^{\frac{i}{\hbar}\hat{H}t}\hat{\rho}(\vec{r})\mathrm{e}^{-\frac{i}{\hbar}\hat{H}t}|\Psi^{N-1}(0)\rangle \\ &= \langle\Psi^{N-1}(t)|\hat{\rho}(\vec{r})|\Psi^{N-1}(t)\rangle, \end{aligned} \tag{2}$$

where $\hat{H}$ is the Hamiltonian of the ionized system.

The cationic state was prepared by the instantaneous removal of an electron from a localized 2*s* orbital of the corresponding site (O or F). This $2s^{-1}$ initial state was propagated with the short iterative Lanczos technique [39, 40], using the full cationic Hamiltonian of the system built via the algebraic diagrammatic construction (ADC) scheme [41] for obtaining the many-body Green's function. Further technical and theoretical information about construction and analysis of the charge density can be found in references [38, 40, 42].

For all calculations and molecules the aug-cc-pVDZ basis set [43] was employed, except for **tfoh-4C**, for which we used the jul-cc-pVDZ basis set, and **tfoh-5C**, for which the DZP basis set was used. The geometries of the molecules in this project were optimized at the MP2 level of theory. The single-ionization spectrum was computed with the non-Dyson ADC(3) method [44], while the ADC(2) method [45, 46] was used to obtain the energetics of the double cation.

Two important points need to be discussed here. First, all calculations have been performed at a fixed geometry. The impact of nuclear motion on pure electron dynamics has been

studied in the case of charge migration, especially for the time span of electron coherence. Nuclear motion has been shown to affect electron coherence on a time scale of a few femtoseconds to more than 10 fs, depending on the system [47–50]. As we will see, the non-local decays studied here culminate within only a few femtoseconds, and therefore the fixed-nuclear approximation should not significantly influence the results. Second, the employed multielectron wave-packet propagation methodology can reliably describe decay processes only if the emitted electron is relatively slow. Faster electrons require specific basis sets [51]. In all of the simulations described in this report, the emitted electrons are slow enough, and no artifact from electron reflection at the edge of the basis space has been observed.

3. Results

As a starting point for understanding the processes studied, the calculated ionization (IP) and double-ionization (DIP) spectra of the trifluoroalkyl alcohol, **tfoh-3C**, are presented in figure 2.

Each line in the IP spectrum corresponds to a cationic eigenstate. Its position is determined by the corresponding ionization potential, and its spectral intensity, or pole strength, is given by the mono-electronic component of the state, i.e. it reflects the extent of one-hole (1h) contributions to that eigenstate. As the states are normalized, due to the electron correlation the pole strength therefore does not add up to 1. The disparity from a spectral intensity of 1 represents the multi-electronic component of the state, which at the ADC(3) level of theory is described by the weight of all possible two-hole-one-particle (2h1p) configurations contributing to the corresponding state. Analogously, the DIP spectrum consists of lines, with heights determined by the weight of all 2h configurations contributing to the corresponding dicationic eigenstate, and 3h1p configurations are responsible for the disparity from a spectral intensity of 1.

Due to many-body effects, the removal of an electron from a single orbital may result in the population of several or even many states [52]. This is precisely the case with the cationic states beyond 30 eV in figure 2. We see a few clumped groupings of lines, which correspond to ionization out of the relatively localized 2*s* orbitals from either the oxygen or fluorine atoms. The grouping of lines around 35 eV (depicted in red) is populated by the removal of an electron from the $10a'$ molecular orbital, which is mainly constructed from the oxygen 2*s* atomic orbital, while the three groupings of lines at 40 eV and above (depicted in blue, green, and orange) correspond to ionizations out of molecular orbitals that are combinations of the fluorine 2*s* atomic orbitals.

From the DIP spectrum, shown in the lower part of the bottom panel of figure 2, we see that these ionic states lie above the double-ionization threshold (being at about 28 eV) and thus can undergo electronic decay into a doubly ionized state. Since we aim at studying the non-local decay, we are only interested in final states having larger contributions of 2h-configurations with a hole on the oxygen and a hole on the fluorines. The weight of such 2h-configurations in the dicationic states is plotted in purple in the DIP spectrum. It is seen that although

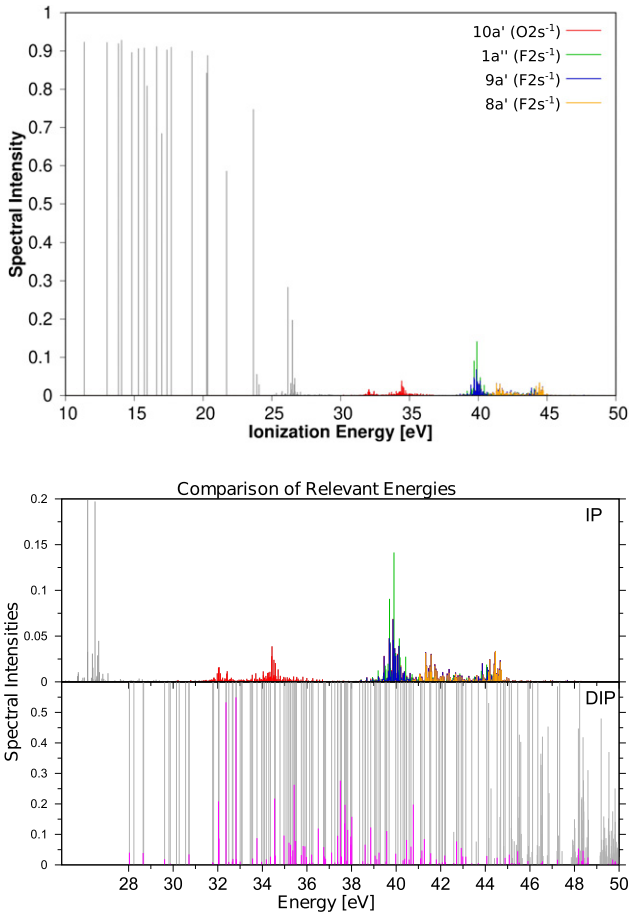

Figure 2. Top: ionization spectrum of **tfoh-3C** computed using the ADC(3) method. Each line represents a cationic eigenstate of the molecule. The states populated by the removal of an electron from the O2*s* orbital are depicted in red, while those corresponding to ionization of each of the three F2*s*-orbitals are shown in green, blue, and orange, respectively. Bottom: comparison of the relevant energy range of the ionization spectrum (IP) and the double-ionization spectrum (DIP) of **tfoh-3C**. The DIP is computed with ADC(2). Each line in the DIP spectrum represents a dicationic eigenstate of the molecule. The contributions to the dicationic states of the configurations with one hole localized on the fluorines and one on the oxygen are depicted in purple.

such 2h-configurations contribute even to the ground dicationic state, the lowest energy states that describe the system with a hole on the oxygen and a hole on the fluorines appear around 32 eV. Therefore, not all of the O($2s^{-1}$) states can decay to such final states, and we can expect the decay to emit very slow electrons, with close to zero kinetic energies. The F($2s^{-1}$) states are higher in energy, and thus their non-local decay will emit few-eV electrons.

Let us now see how these decay processes proceed in time and space.

3.1. Non-local decay after oxygen ionization

The decay can be followed by computing the time-dependent spatial distribution of the hole density, equation (1), after the removal of an O2*s* electron. In the case of quasi-linear

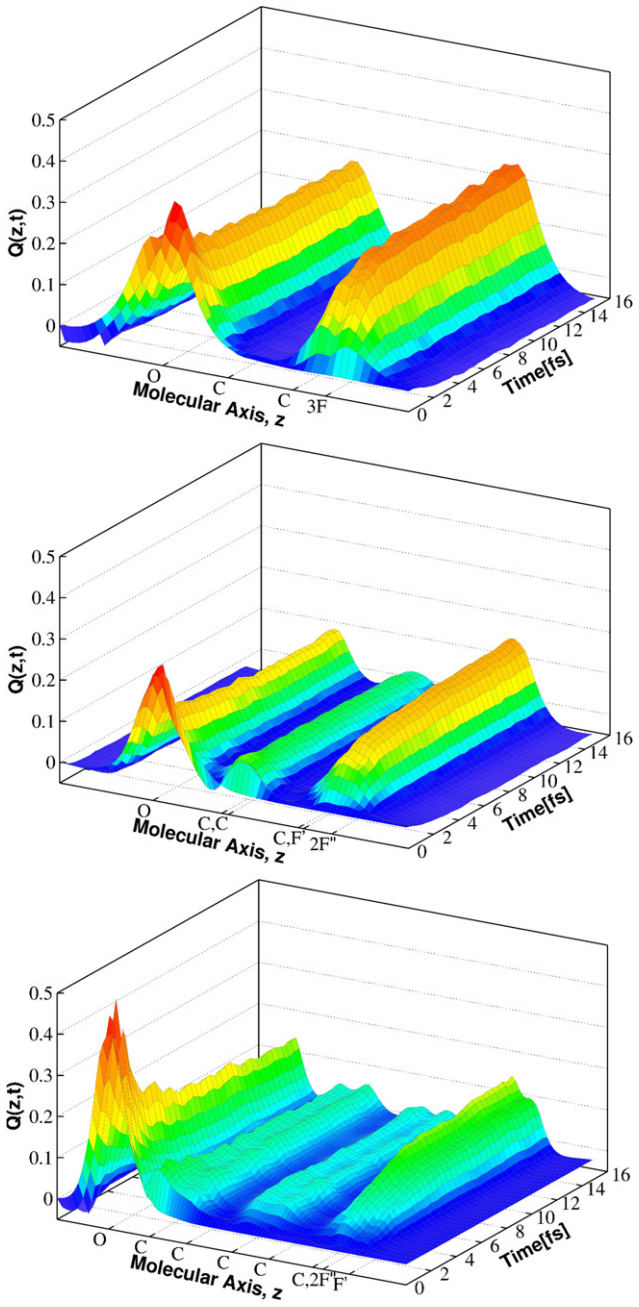

Figure 3. Evolution of the hole density $Q(z,t)$ following ionization of the O2*s* orbital along the molecular axis z. From top to bottom, the plots are provided for **tfoh-2C**, **tfoh-3C**, and **tfoh-5C**. The opening of the second hole on the fluorines is clearly observed.

molecules, this can be conveniently represented by integrating $Q(\vec{r},t)$ over two of the spatial dimensions perpendicular to the molecular axis z, which is oriented along the carbon chain. The obtained $Q(\vec{z},t)$ are shown in figure 3 for three of the trifluoroalkyl alcohol molecules investigated in the present study—**tfoh-2C**, **tfoh-3C**, and **tfoh-5C**.

It can be seen that the evolution of the hole density is very similar in all the cases. In the beginning, the hole is localized on the oxygen (the initial 2*s* vacancy), and as time proceeds, a second hole is gradually opened on the fluorines. Although not evident from figure 3, as we will see, the hole on the oxygen also undergoes a change in its character, reflecting the process of filling the initial 2*s* vacancy with a higher-lying electron of the oxygen or the carbon chain. The longer the chain, the slower the non-local decay, but even in **tfoh-5C**, it is extremely fast and takes only a few femtoseconds. Note that the evolution of the hole density reflects all decay channels of the O2*s* vacancy. For example, the hole density that builds up on the carbon atoms along the chain, clearly visible in the **tfoh-3C** and **tfoh-5C** cases in figure 3, is a result of decay channels that involve the bridge electrons. From the analysis of this density evolution, we know that those channels are comparable or even slightly faster than the decay ejecting fluorine electron, but a reliable calculation of the corresponding branching ratios is not possible with the present method.

Using the molecular orbitals (MOs) of the neutral molecule as a basis, the hole density can be represented as [38]

$$Q(\vec{r},t) = \sum_p |\tilde{\varphi}_p(\vec{r},t)|^2 \tilde{n}_p(t), \tag{3}$$

where $\tilde{\varphi}_p(\vec{r},t)$ are the so-called natural charge orbitals, and $\tilde{n}_p(t)$ are their hole-occupation numbers. As the name suggests, the hole-occupation number describes the fraction of the hole charge which is in the corresponding natural charge orbital at a given time, while at each time point, the natural charge orbitals consist of different linear combinations of the neutral molecular orbitals. The hole occupations can be both positive and negative numbers, depending on, respectively, whether an electron is removed from an initially occupied orbital (a hole is created), or an electron is created in a virtual orbital (a particle is created). This representation of the hole density allows for a detailed analysis of the decay dynamics.

As an example, let us now take a closer look at the decay in **tfoh-1C**. The hole density and the dominant natural charge orbitals bearing the holes and the particle are plotted in figure 4. At time $t = 0$, 100% of the hole lies in the O2*s* orbital. By 0.4 fs later, we see that this orbital now contributes to only about 21% of the hole density, while two other orbitals with O2*p* character have been populated. This reveals the most efficient deexcitation channel of the initial vacancy—a local $2p \rightarrow 2s$ transition on the oxygen. By 0.8 fs, the initial O2*s* orbital is no longer the dominant orbital of the hole density, and orbitals having strong fluorine character start to contribute, indicative of the process of the second hole opening on the fluorines, from where the decay electron is ejected. Typically, the outgoing electron is described by a large number of charge orbitals, constructed by diffuse virtual MOs, and this is why a detailed analysis is complicated to show pictorially. However, for completeness, in figure 4 we include the natural charge orbital bearing the largest fraction of the emitted electron.

3.2. Comparison of O($2s^{-1}$) decay in **tfoh** *and* **cume** *systems*

As we saw, the evolution of the hole density contains detailed information on all decay channels of the O($2s^{-1}$) state. The time constant of the non-local decay channels can be extracted by fitting the accumulation of hole density around the fluorine atoms with an exponential function [33]. Employing this

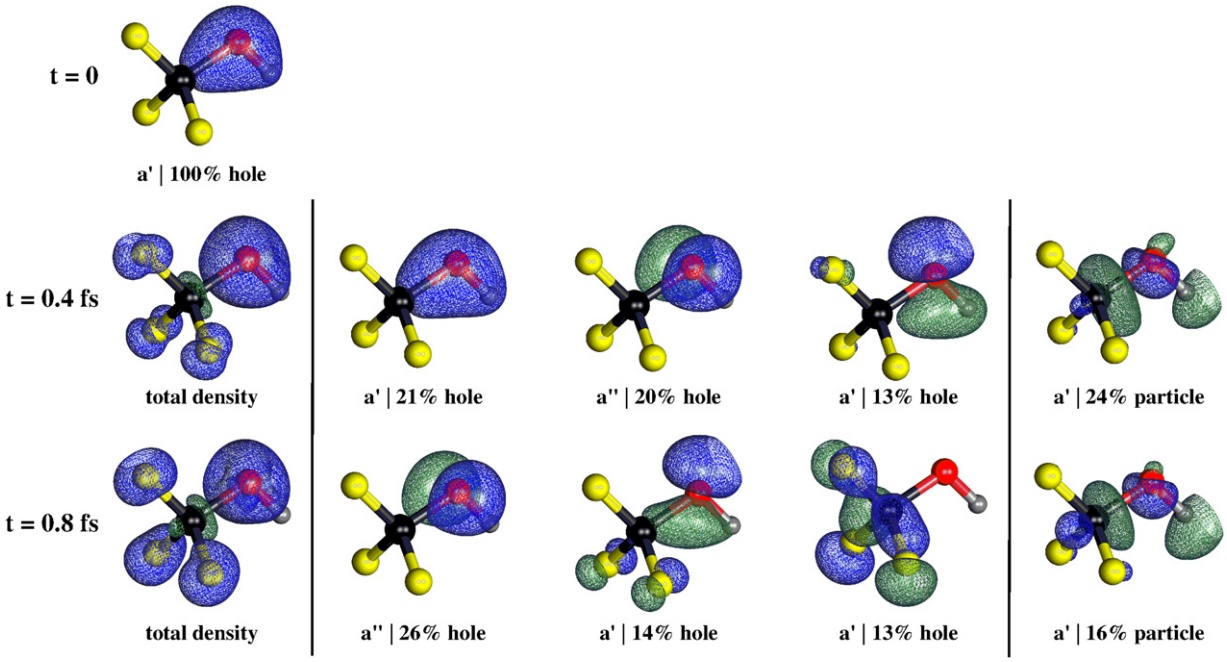

Figure 4. Analysis of the early time evolution of the hole density after creating a hole in the O2*s* orbital in **tfoh-1C**. Snapshots of the total hole density (left) and the dominant hole and particle charge orbitals that contribute to it are shown at times 0.4 fs and 0.8 fs. It is clearly seen how the initial hole changes from O2*s* character into O2*p* character, reflecting the main electron transitions filling the initial vacancy, and a second hole opening on the fluorines. A small fraction of negative hole density, or an excess of electrons, builds up on the carbon and is depicted in green in the total density snapshots.

technique, it was found in our recent study of the difluorocumulenone systems [33] that the decay time increases almost linearly with the distance between the final hole sites. A similar trend was found for the trifluoroalkyl alcohols, as seen in figure 5. The time constants are also fairly similar in magnitude in both molecular families, suggesting that non-linearity and the saturation of the carbon bridge are not significant factors in the efficiency of energy transfer, although the decay time in the **tfoh** systems seems to increase slightly slower with distance.

Another interesting observation is that the difluorocumulenones exhibit odd–even effects, while the trifluoroalkyl alcohols show practically no dependence on the parity of the number of carbon atoms in the bridge. We see that the non-local decay in difluorocumulenones with an odd number of carbon atoms tends to proceed somewhat faster, and that in systems with an even number of carbons somewhat slower, than the overall trend for a particular distance between oxygen and fluorine atoms. For the trifluoroalkyl alcohols, such variation in the decay time evolution is barely visible. Odd–even effects in cumulenic systems have been previously reported in the literature [53]. It has been observed that various properties, such as electronic structure, bond length, and structural stability can alter with the parity of the number of carbons. This has been explained by the distinct π-conjugation of even and odd structures. In the even-numbered carbon chain, one of the π-systems of the *sp* carbon framework spans the whole length of the bridge and can conjugate with both terminal groups, while in the odd-numbered carbon chain, each of the orthogonal π-systems conjugate with only one of the terminal groups [53], which might also be the reason for the different efficiency in the energy transfer through the bridge. We will return to this point below.

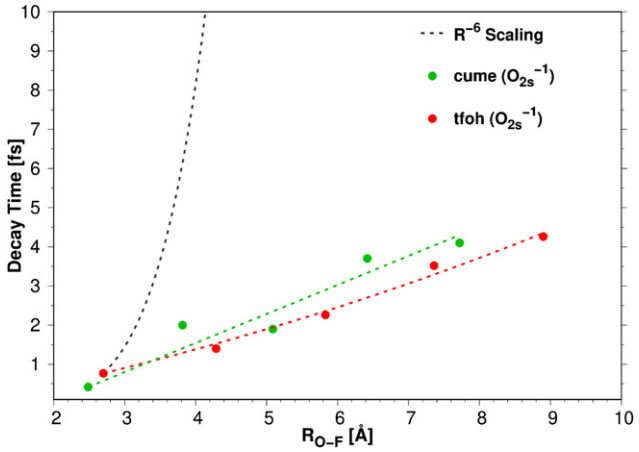

Figure 5. Non-local decay times of the O($2s^{-1}$) state in **tfoh** and **cume** systems as a function of O–F distance. Time constants for the **cume** system, taken from reference [33], are plotted with green dots, while those of **tfoh** with red dots. Linear fits to those points are shown in green and red dashed lines, respectively. An R^{-6} scaling, expected for non-local decay through empty space, is plotted with the gray dashed curve for comparison.

3.3. *Non-local decay after fluorine ionization*

Let us now examine the possibility of a non-local electronic decay initiated by ionization of the fluorines, i.e. to study the efficiency of energy transfer through the bridge in the opposite

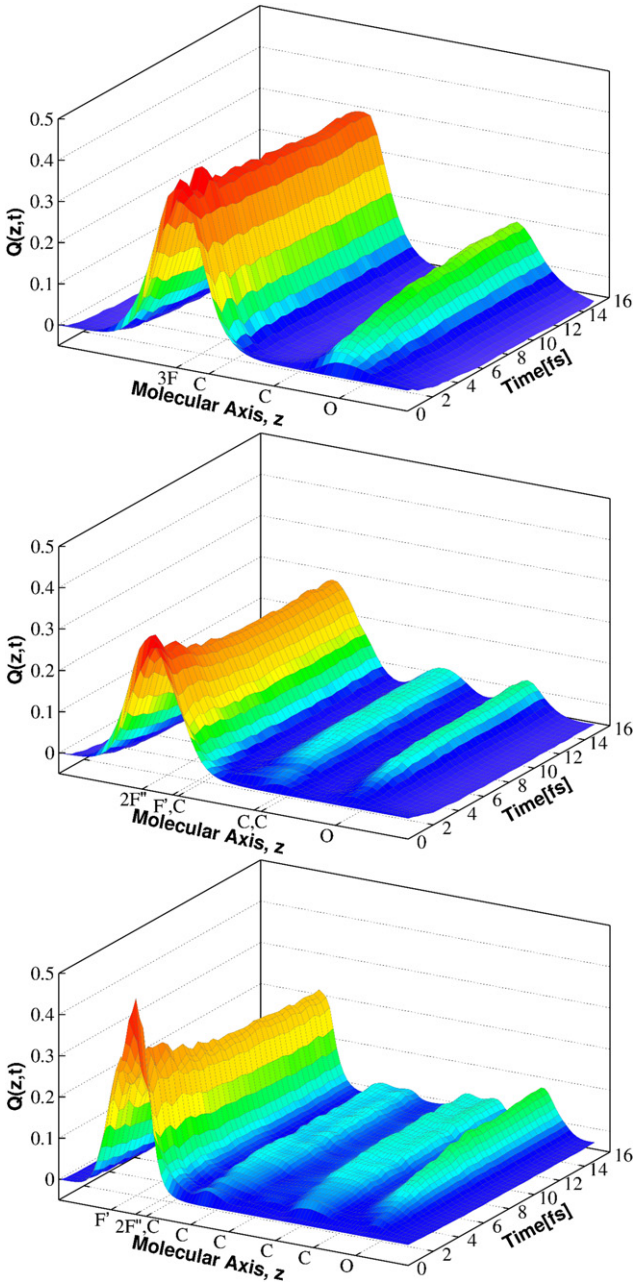

Figure 6. Evolution of the hole density $Q(z, t)$ following ionization of the deepest F2*s* orbital along the molecular axis z. From top to bottom, the plots are provided for **tfoh-2C**, **tfoh-3C**, and **tfoh-5C**. Note that the orientation of the molecular axis has been inverted compared to figure 3. The opening of the second hole on the oxygen is clearly seen; however, the decay channels involving the carbon chain and the local decay within the fluorines are rather pronounced.

direction. There are three possible F2*s* molecular orbitals available for initial ionization, which all trigger very similar decay dynamics. The hole density evolution initiated by ionization of the energetically deepest-lying F2*s* orbital (populating the group of states depicted in orange in figure 2 for **tfoh-3C**) is provided in figure 6. Note that for clarity, the orientation of the molecular axis has been inverted compared to figure 3.

In general, we see that the non-local decay, emitting an electron from the oxygen, is less pronounced and slower compared

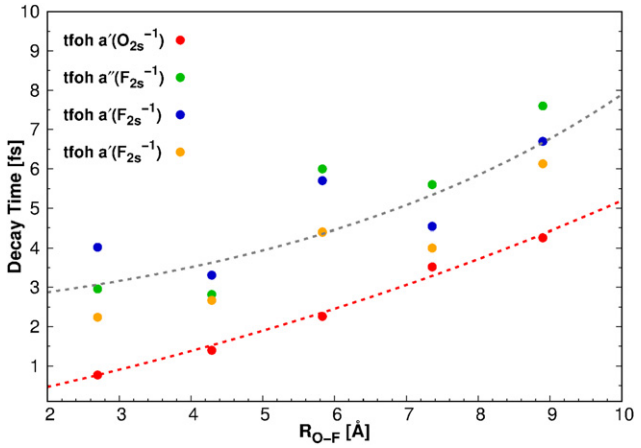

Figure 7. Comparison of the non-local decay time constants as a function of the distance between the involved O and F sites. The lifetimes of the O($2s^{-1}$) state are depicted in red, while those of the three different F($2s^{-1}$) states in green, blue, and orange, respectively. For the color-coding of the fluorine states, refer to legend of figure 2.

to the process initiated by the O($2s^{-1}$) state. This is due to the fact that the F($2s^{-1}$) state is higher in energy and more decay channels involving the carbon chain are energetically accessible. Moreover, the very efficient local Auger decay, emitting an electron from the fluorines, is also open. In spite of this competition, the non-local decay to the oxygen remains highly efficient and proceeds in just a few femtoseconds.

It is interesting to compare the lifetimes of the non-local decays initiated on opposite ends, as this reveals information on the correlation between the oxygen and fluorine electrons mediated by the carbon chain. This can be also interpreted as the efficiency of the energy transfer through the chain in both directions: O $\rightarrow$ F and F $\rightarrow$ O. Such a comparison is shown in figure 7 for the O($2s^{-1}$) decay and the processes initiated by the three F($2s^{-1}$) states. It is seen that the decay initiated by a hole on the oxygen proceeds approximately 2–3 times faster than a decay initiated by a fluorine vacancy. The increase of the decay time with distance, however, follows a similar trend in both cases; namely, the increase is nearly linear.

Several factors might play a role in slowing the non-local decay of the F($2s^{-1}$) states. The efficiency of the non-local decay depends on the transition filling the initial vacancy, the energy transfer to the opposite end of the molecule, and the transition ejecting the electron into the continuum. At lowest-order perturbation theory, the efficiency of the decay, or the decay width, is proportional to the modulus-square of the Coulomb repulsion matrix element connecting the two involved electrons [54]. The efficiency, therefore, depends on the overlap between the orbitals describing the initial and final states of the two electrons. As the transition to the continuum is not expected to be very different between the two non-local decays, the reason for the slower F($2s^{-1}$) decay most likely is due to the fact that the F2*s* electrons lie energetically deeper within the electronic shell, and thus the F2*s* orbitals are more localized compared to the O2*s* orbital. Accordingly, the overlap between the spatially extended valence orbitals and the more localized F2*s* vacancy is smaller, which will result in a longer decay time.

Meanwhile, the energy transfer through the chain strongly depends on the amount of energy to be transmitted. If the energy is in resonance with some excitonic state of the chain, the transfer will be very efficient. A similar effect has already been reported for non-bound and inert mediators of a non-local electronic decay—the so-called superexchange ICD mechanism [55, 56], where the presence of a helium atom between two distant neons is shown to increase the $Ne^{+}(2s^{-1})Ne$ ICD rate sixfold. In our case, when the bridge is bound to the decaying species and not inert (i.e. it can also participate in the decay), the situation is more complex. It becomes quite difficult to identify excited states on the chain that might enhance the energy transmission, or in other words, to enhance the correlation between the fluorine and oxygen electrons directly participating in the decay. The difference in the efficiency of energy transfer for $F \rightarrow O$ compared to $O \rightarrow F$ could, however, partially be due to an energy mismatch between the transition filling the initial vacancy and a particular excitation of the chain.

Another interesting difference in the non-local decays of $O(2s^{-1})$ and $F(2s^{-1})$ is that the latter exhibits odd–even effects; while, as we saw already, they do not appear in the relaxation of the O2*s* vacancy. As seen from figure 7, the evolution of the non-local decay time of the $F(2s^{-1})$ state with the bridge length clearly shows a zig–zag pattern, while practically no variation is observed in the $O(2s^{-1})$ case. It seems, therefore, that the energy transfer through the bridge depends on the directionality of the energy flow. The efficiency of a non-local decay, however, does not depend only on the energy transfer between the two involved sites, but is a result of a rather complicated interplay between the local transitions and their coupling through the bridge electrons. The alternating structural differences in the even and odd trifluoroalkyl alcohols systematically modify only certain parts of their energetics. This may affect only the excitations that influence the non-local decay of the $F(2s^{-1})$ state, and not those involved in the $O(2s^{-1})$ relaxation in the same way, resulting in different resonance enhancement conditions in the O2*s* and F2*s* cases. Additionally, we observe odd–even effects in valence orbitals with significant localization around the fluorine atoms, which correspondingly would affect the transitions filling the F2*s* vacancy to a greater degree. We note, however, that a thorough investigation is needed to understand why the odd–even effects appear only in the non-local decay of the fluorine vacancy and not in that of the oxygen.

4. Conclusions

Using the multielectron wave-packet propagation method, we have shown that the non-local decay of O2*s* states in trifluoroalkyl alcohols proceeds with a similarly high efficiency to that in the difluorocumulenones reported earlier. In addition, we obtained a very similar functional dependence of the increase of the lifetime on the distance between the oxygen and the fluorines in the two molecular families. This confirms the previously reported observation that the decay proceeds more efficiently through a molecular bridge than through empty space. Our results also suggest that the linearity of the bridge does not play a significant role in the decay efficiency, although we obtain a slightly faster decay through a saturated chain.

Our calculations also show that the non-local decay can proceed in the opposite direction; i.e. a 2*s* hole in the fluorines can decay by emitting an electron from the oxygen. While still highly efficient, the fluorine-initiated decay is systematically slower compared to the oxygen-initiated decay, which may be due to both the more localized initial hole as well as the different resonant conditions between the two deexcitation transitions and a corresponding excitation of the chain. The influence of such resonant mechanisms on the efficiency of the energy transfer, however, must be more thoroughly investigated. A detailed review on the type of the relevant excitonic states and their energetics could provide important insight and ultimately allow for the design of efficient bridges and functional groups.

Before concluding, we would like to touch upon the possible experimental observation of such dynamics. The ultrafast timescale of the decay dynamics certainly presents an experimental challenge. Moreover, the non-local decay is only one of the possible relaxation channels of the initial state of interest, which together with the involved vibrational structure expected in the spectra makes the use of frequency domain techniques and linewidth analysis nearly impossible. A promising alternative is offered by attosecond spectroscopy. The initial state can be created by an ultrashort XUV pulse and its evolution probed either by streaking with a delayed IR pulse [57] or by transient absorption with a delayed XUV pulse [58]. Both techniques have been successfully applied to trace in real time few-femtosecond decay dynamics in atoms. Due to the much higher density of states in molecules, transient absorption seems a better technique for the present case, as it offers a higher spectral resolution. The evolution of absorption lines corresponding to $2s \rightarrow 2p$ transitions on O or F could be monitored to unambiguously trace the non-local decay. We hope that the present study will stimulate such experiments.

Acknowledgments

Financial support by the DFG is gratefully acknowledged. AIK thanks US ARO (Grant No. W911NF-14-1-0383) and ERC (AdG No. 692657) for financial support.

ORCID iDs

Victor Despré https://orcid.org/0000-0001-7364-5625
Alexander I Kuleff https://orcid.org/0000-0003-2583-4370

References

[1] Lépine F, Ivanov M Y and Vrakking M J 2014 *Nat. Photon.* **8** 195
[2] Nisoli M, Decleva P, Calegari F, Palacios A and Martín F 2017 *Chem. Rev.* **117** 10760
[3] Kling M *et al* 2006 *Science* **312** 246

[4] Klünder K *et al* 2011 *Phys. Rev. Lett.* **106** 143002
[5] Neidel C *et al* 2013 *Phys. Rev. Lett.* **111** 033001
[6] Calegari F *et al* 2014 *Science* **346** 336
[7] Kraus P M *et al* 2015 *Science* **350** 790
[8] Belshaw L, Calegari F, Duffy M J, Trabattoni A, Poletto L, Nisoli M and Greenwood J B 2012 *J. Phys. Chem. Lett.* **3** 3751
[9] Marciniak A *et al* 2015 *Nat. Commun.* **6** 7909
[10] Galbraith M *et al* 2017 *Nat. Commun.* **8** 1018
[11] Galbraith M *et al* 2017 *Phys. Chem. Chem. Phys.* **19** 19822
[12] Marciniak A *et al* 2018 *J. Phys. Chem. Lett.* **9** 6927
[13] Marciniak A *et al* 2019 *Nat. Commun.* **10** 337
[14] Auger P 1925 *J. Phys. Radium* **6** 205
[15] Åberg T 1982 *Handbuch der Physik: Corpuscles and Radation in Matter I* (Berlin: Springer)
[16] Coster D and Kronig R d L 1935 *Physica* **2** 13
[17] Guillot C, Ballu Y, Paigné J, Lecante J, Jain K, Thiry P, Pinchaux R, Petroff Y and Falicov L 1977 *Phys. Rev. Lett.* **39** 1632
[18] Bambynek W, Crasemann B, Fink R, Freund H-U, Mark H, Swift C, Price R and Rao P V 1972 *Rev. Mod. Phys.* **44** 716
[19] Krause M O and Oliver J 1979 *J. Phys. Chem. Ref. Data* **8** 329
[20] Cederbaum L, Zobeley J and Tarantelli F 1997 *Phys. Rev. Lett.* **79** 4778
[21] Santra R and Cederbaum L S 2002 *Phys. Rep.* **368** 1
[22] Stoychev S D, Kuleff A I and Cederbaum L S 2011 *J. Am. Chem. Soc.* **133** 6817
[23] Averbukh V *et al* 2011 *J. Electron. Spectrosc. Relat. Phenom.* **183** 36
[24] Gokhberg K, Kolorenč P, Kuleff A I and Cederbaum L S 2014 *Nature* **505** 661
[25] Jahnke T *et al* 2004 *Phys. Rev. Lett.* **93** 163401
[26] Öhrwall G *et al* 2004 *Phys. Rev. Lett.* **93** 173401
[27] Morishita Y *et al* 2006 *Phys. Rev. Lett.* **96** 243402
[28] Mucke M *et al* 2010 *Nat. Phys.* **6** 143
[29] Trinter F *et al* 2014 *Nature* **505** 664
[30] Jahnke T 2015 *J. Phys.* B **48** 082001
[31] Matthew J and Komninos Y 1975 *Surf. Sci.* **53** 716
[32] Averbukh V, Müller I B and Cederbaum L S 2004 *Phys. Rev. Lett.* **93** 263002
[33] Kuleff A I 2017 *Chem. Phys.* **482** 216
[34] Cederbaum L S and Zobeley J 1999 *Chem. Phys. Lett.* **307** 205
[35] Kuleff A I and Cederbaum L S 2014 *J. Phys. B: At. Mol. Opt. Phys.* **47** 124002
[36] Despré V and Kuleff A I 2019 *Theor. Chem. Acc.* **138** 110
[37] Xiang D, Wang X, Jia C, Lee T and Guo X 2016 *Chem. Rev.* **116** 4318
[38] Breidbach J and Cederbaum L 2003 *J. Chem. Phys.* **118** 3983
[39] Leforestier C *et al* 1991 *J. Comp. Phys.* **94** 59
[40] Kuleff A I, Breidbach J and Cederbaum L S 2005 *J. Chem. Phys.* **123** 044111
[41] Schirmer J 2018 *Many-Body Methods for Atoms, Molecules and Clusters* vol 94 (Berlin: Springer)
[42] Breidbach J and Cederbaum L 2007 *J. Chem. Phys.* **126** 034101
[43] Dunning T H Jr 1989 *J. Chem. Phys.* **90** 1007
[44] Schirmer J, Trofimov A B and Stelter G 1998 *J. Chem. Phys.* **109** 4734
[45] Schirmer J and Barth A 1984 *Z. Phys.* A **317** 267
[46] Tarantelli F 2006 *Chem. Phys.* **329** 11
[47] Despré V, Marciniak A, Loriot V, Galbraith M, Rouzée A, Vrakking M, Lépine F and Kuleff A 2015 *J. Phys. Chem. Lett.* **6** 426
[48] Vacher M, Bearpark M J, Robb M A and Malhado J P 2017 *Phys. Rev. Lett.* **118** 083001
[49] Arnold C, Vendrell O and Santra R 2017 *Phys. Rev.* A **95** 033425
[50] Despré V, Golubev N V and Kuleff A I 2018 *Phys. Rev. Lett.* **121** 203002
[51] Kuleff A I and Cederbaum L S 2007 *Phys. Rev. Lett.* **98** 083201
[52] Cederbaum L, Domcke W, Schirmer J and Von Niessen W 1986 *Adv. Chem. Phys.* **65** 115
[53] Januszewski J and Tykwinski R 2014 *Chem. Soc. Rev.* **43** 3184
[54] Santra R, Zobeley J and Cederbaum L S 2001 *Phys. Rev.* B **64** 245104
[55] Miteva T, Kazandjian S, Kolorenč P, Votavová P and Sisourat N 2017 *Phys. Rev. Lett.* **119** 083403
[56] Votavová P, Miteva T, Engin S, Kazandjian S, Kolorenč P and Sisourat N 2019 *Phys. Rev.* A **100** 022706
[57] Drescher M *et al* 2002 *Nature* **419** 803
[58] Hütten K *et al* 2018 *Nat. Commun.* **9** 719